THz Polarizer Controller Based on Cylindrical Spoof Surface Plasmon Polariton (C-SSPP)

Mahdi Aghadjani and Pinaki Mazumder, *Fellow, IEEE*

***Abstract*—Spoof surface plasmon polariton (SSPP) based devices have recently garnered a great deal of attention owing to their ability to propagate THz signal without dispersion and very low signal attenuation. In this paper, a rigorous mathematical model has been proposed by performing full-field analysis on the periodically corrugated cylindrical waveguide. It has been shown that this structure has the capability of propagating localized spoof surface plasmons polariton (SSPP) mode of EM waves. The variation of band diagrams as a function of different groove dimensions has been investigated. Finally, by employing cylindrical SSPP a new polarizer controller has been designed that can be utilized to design THz Boolean gates.**

***Index Terms*—Dispersion relation, spoof surface plasmon polariton (SSPP), polarization, full-field analysis, anisotropic material.**

I. Introduction

THERE has been much interest in developing terahertz (THz) components and circuits in recent years as a result of their applications in several emerging areas such as biomedical sensing and imaging, ultrafast computer circuits, astronomical remote sensing, and hazardous chemical detection [1]–[4]. Also for passive THz devices, design and fabrication of guiding structures, focusing elements and frequency selective filters have gained considerable attention [5]–[7]. In addition, in the optical frequency range there has been extensive research on development of plasmonic devices as a result of the possibility of miniaturization of optical devices below the diffraction limit.

Surface plasmons result from the oscillation of plasma along the interface of metal and dielectric. It happens as a result of negative dielectric of certain metal below the plasma frequency. There have been some theoretical and experimental works to utilize these modes in a frequency range of 0.3–10 THz [9]–[11]. Besides, there are efforts that utilize conventional waveguides such as metallic wires, tubes, index-guiding silicon slab waveguides or sapphire fibers, etc. Unfortunately, the conventional metallic tube waveguides are not suitable because of high loss. Si waveguides are not flexible and some waveguides, such as sub-wavelength metal wire, has high bending loss and coupling difficulty [5], [12]–[15]. A newly developed method to overcome the group velocity dispersion of terahertz wave and weak guiding at THz frequencies is the utilization of spoof surface palasmon polariton (SSPP) waves confined to the periodically corrugated metallic structures [16]–[19].

These SSPP modes exhibit features such as field enhancement and localization. In this technique the transverse mode of SSPP follow the same behavior of surface plasmons at interface of metal dielectric at optical frequencies. It has been first shown by Wang *et al.* that it is possible to have dispersion-less propagation along metallic wire surrounded by dielectric at THz frequency [17]. Later Pendry *et al.* proposed a periodic structure containing grooves at metallic dielectric interface to support THz propagation [18].

As long as the periodicity and dimensions of the resonators are much smaller than the wavelength of operation, it is possible to replace the corrugated conducting structure with a metal whose plasma frequency depends on the depth of the grooves. This is the reason that the term 'spoof surface plasmons' used for the confined surface waves propagating along the corrugated perfectly-conducting surface [24].

In [20]–[22], the corrugated SSPP structures have been realized by placing rectangular resonator along the propagation path of rectangular waveguide and the parallel plate waveguide.

In our work, by inserting periodic grooves along the direction of propagation in a cylindrical waveguide, a corrugated SSPP waveguide has been constructed. This structure shows strong confinement of electromagnetic energy inside the grooves near their resonant frequency. This property makes it applicable in narrowband THz circuits such as filter or active switches or polarizer rotators. Similar structures have been studied in other research groups such as [8] and [23], but this structure compared to [23] is conjugated. By applying special materials into the circular SSPP waveguide, for example, anisotropic dielectric, the polarization state of the THz travelling wave, will be preferably selected at input and will evolve while propagating. If, in addition, we can control the refractive indices through external stimuli, we can accommodate the output polarization of the THz signal to our needs.

The paper is organized as follows. In Section II, a full-field analysis of cylindrical SSPP structure has been performed and a mathematical equation for dispersion diagram has been derived. In Section III, a comparison between our numerical results and HFSS result is made and a discussion on the variation of the band diagrams of the SSPPs as a function of the geometrical parameters of the structure is done. In Section IV, a polarizer rotator based on our cylindrical SSPP waveguide is proposed.

II. Calculation of Dispersion Diagram

The structure under investigation consists of a dielectric cylindrical part covered by perfectly conducting surface. As

Manuscript received February 26, 2014; revised October 10, 2014 and December 23, 2014; accepted May 09, 2015. Date of publication July 08, 2015; date of current version July 16, 2015. This work was supported in part by a National Science Foundation under Grant NSF 1116040.

The authors are with the Department of Electrical Engineering and Computer Science, University of Michigan, Ann Arbor, MI 48109 USA (e-mail: mazum@eecs.umich.edu).

Color versions of one or more of the figures in this paper are available online at http://ieeexplore.ieee.org.

Digital Object Identifier 10.1109/TTHZ.2015.2439677

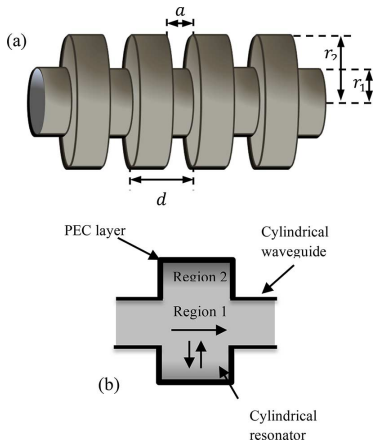

Fig. 1. (a) Schematic view of the corrugated cylindrical waveguide. (b) Unit cell of the structure.

mentioned before, the proposed SSPP structure is a periodic device. In order to calculate the dispersion relationship, electromagnetic fields need to be calculated in one period. Fig. 1 shows the overall view of SSPP waveguide and the unit cell of structure. As can be seen, one period of waveguide has been divided into two regions. Region 1 acts as a cylindrical waveguide, while Region 2 is a cylindrical resonator.

In our convention, d is the period of the grooves, a and R_2 represent the width and radius of the grooves, while R_1 is the radius of the smooth part of the waveguide. Moreover the permittivity of Region 1 and grooves can be denoted by n. Based on Maxwell's equations, mathematical expressions of the TM-polarized waves propagating in z direction along grooves are explicitly written out for both Regions 1 and 2. To this goal, the magnetic and electric vector potentials in Region 1 can be assumed as $A_1 = \psi_{1a}\hat{z}$ and $F_1 = \psi_{1f}\hat{z}$, where

$$\begin{aligned}\psi_{a1} &= I_N(k_\rho\rho)\cos(N\varphi)e^{-ik_z^m z}\\ \psi_{f1} &= I_N(k_\rho\rho)\sin(N\varphi)e^{-ik_z^m z}.\end{aligned} \tag{1}$$

In (1), $I_N(k_\rho\rho)$ is the modified Bessel function of the first kind. As is common in solving Maxwell equations in periodic structures, the EM field can be best represented by a Bloch–Floquet mode expansion. k_z^m, therefore, denotes the wavevector of mth-order Bloch–Floquet mode along z-axis and is expressed by

$$k_z^m = k_z + \frac{2m\pi}{L}. \tag{2}$$

Similarly, the magnetic vector potential in Region 2 is assumed to be a vector along the z -axis as expressed by $A_2 = \psi_{2a}\hat{z}$ and $F_2 = \psi_{2f}\hat{z}$, in which

$$\begin{aligned}\psi_{a2} &= \left(A^+H_N^2(k_{\rho_2}\rho) + A^-H_N^1(k_{\rho_2}\rho)\right)\cos(N\varphi)\cos\left(\frac{n\pi}{a}z\right)\\ \psi_{f2} &= \left(B^+H_N^2(k_{\rho_2}\rho) + B^-H_N^1(k_{\rho_2}\rho)\right)\sin(N\varphi)\sin\left(\frac{n\pi}{a}z\right).\end{aligned} \tag{3}$$

The term $\cos((n\pi)/(a)z)$ and $\sin((n\pi)/(a)z)$ is included in the expression in order to guarantee that E_ρ vanishes at $z = a$ inside the resonators. The fields are assumed as upward and downward waves, and $H_N^{1,2}(k_{\rho_2}\rho)$ are Hankel functions of the first and second kind, respectively

$$\begin{aligned}H_N^2(\rho) &= J_N(\rho) - iN_N(\rho)\\ H_N^1(\rho) &= J_N(\rho) + iN_N(\rho).\end{aligned} \tag{4}$$

Having the electric and magnetic vector potential in both regions EM field components can be calculated as follows:

$$\begin{aligned}D &= \frac{1}{i\omega}\nabla\times\nabla\times\vec{A} - [\varepsilon]\nabla\times\vec{F}\\ H &= \frac{1}{i\omega\mu}\nabla\times\nabla\times\vec{F} + \nabla\times\vec{A}\end{aligned} \tag{5}$$

where $[\varepsilon]$ is a function refractive index of dielectric. We can write D- and H-fields in both regions. For the TM_z modes D- and H-fields are, as follows, as shown in (6) and (7) at the bottom of the page.

Region 1:

$$\begin{bmatrix}D_\rho\\ D_\varphi\\ D_z\end{bmatrix} = \sum_{m=-M}^{M}\begin{bmatrix}-A_m\frac{k_z}{\omega}k_\rho J_N'(k_\rho\rho)\cos(N\varphi)e^{-ik_z^m z}\\ A_m\frac{k_z}{\omega\rho}k_z J_N(k_\rho\rho)\sin(N\varphi)e^{-ik_z^m z}\\ \frac{A_m}{\omega}\left(k^2 - K_z^2\right)J_N(k_\rho\rho)\cos(N\varphi)e^{-ik_z^m z}\end{bmatrix}$$
$$\begin{bmatrix}H_\rho\\ H_\varphi\\ H_z\end{bmatrix} = \sum_{m=-M}^{M}\begin{bmatrix}A_m\frac{-N}{\rho}J_N(k_\rho\rho)\sin(N\varphi)e^{-ik_z^m z}\\ -A_m k_\rho J_N'(k_\rho\rho)\cos(N\varphi)e^{-ik_z^m z}\\ 0\end{bmatrix} \tag{6}$$

Region 2:

$$\begin{bmatrix}D_\rho\\ D_\varphi\\ D_z\end{bmatrix} = \begin{bmatrix}\frac{1}{i\omega\varepsilon}\frac{n\pi}{a}k_{\rho_2}\left(\mathrm{A}^+H_N^{2'}(k_{\rho_2}\rho) + \mathrm{A}^-H_N^{1'}(k_{\rho_2}\rho)\right)\cos(N\varphi)\cos\left(\frac{n\pi}{a}z\right)\\ \frac{1}{i\omega\varepsilon\rho}\frac{n\pi}{a}\left(\mathrm{A}^+H_N^2(k_{\rho_2}\rho) + \mathrm{A}^-H_N^1(k_{\rho_2}\rho)\right)\cos(N\varphi)\sin\left(\frac{n\pi}{a}z\right)\\ \frac{1}{i\omega\varepsilon}\left(k^2 - \left(\frac{n\pi}{a}\right)^2\right)\left(\mathrm{A}^+H_N^2(k_{\rho_2}\rho) + \mathrm{A}^-H_N^1(k_{\rho_2}\rho)\right)\cos(N\varphi)\cos\left(\frac{n\pi}{a}z\right)\end{bmatrix}$$
$$\begin{bmatrix}H_\rho\\ H_\varphi\\ H_z\end{bmatrix} = \begin{bmatrix}\frac{-N}{\rho}\left(\mathrm{A}^+H_N^2(k_{\rho_2}\rho) + \mathrm{A}^-H_N^1(k_{\rho_2}\rho)\right)\sin(N\varphi)\cos\left(\frac{n\pi}{a}z\right)\\ -ik_\rho\left(\mathrm{A}^+H_N^{2'}(k_{\rho_2}\rho) + \mathrm{A}^-H_N^{1'}(k_{\rho_2}\rho)\right)\cos(N\varphi)\cos\left(\frac{n\pi}{a}z\right)\\ 0\end{bmatrix} \tag{7}$$

For the TE_z modes the D- and H-fields can be written as (8) and (9) on the page.

Now that the full field expressions are derived, the boundary conditions for tangential fields at the interface of Regions 1 and 2 need to be satisfied. As $a \ll 1$ the only modes that can propagate in the grooves are the fundamental modes with $n = 0$ for TM_z and $n = 1$ for TE_z. We can now implement the boundary conditions for D- and H-fields. Writing the boundary condition for D_z and H_z can be further transcribed as

$$\begin{aligned}\sum_{m=-M}^{m=M} -B_m\left(k_0^2 - k_z^{m^2}\right) I_N(k_\rho R_1) e^{-ik_z^m z} \\ = \left(k_0^2 - \left(\frac{\pi}{a}\right)^2\right)\left(\mathrm{B}^+ H_N^2(k_{\rho_2} R_1)\right. \\ \left. +\mathrm{B}^- H_N^1(k_{\rho_2} R_1)\right) \sin\left(\frac{\pi}{a} z\right)\end{aligned} \tag{10}$$

$$\begin{aligned}\sum_{m=-M}^{m=M} A_m\left(k_0^2 - k_z^{m^2}\right) I_N(k_\rho R_1) e^{-ik_z^m z} \\ = k_0^2\left(\mathrm{A}^+ H_N^2(k_{\rho_2} R_1) + \mathrm{A}^- H_N^1(k_{\rho_2} R_1)\right).\end{aligned} \tag{11}$$

In addition, at $\rho = R_2$ the tangential electric field should vanish. Therefore we have: $A^+ H_N^2(k_{\rho_2} R_2) = A^- H_N^1(k_{\rho_2} R_2)$ and $B^+ H_N^{2'}(k_{\rho_2} R_2) = B^- H_N^{1'}(k_{\rho_2} R_2)$. Then we only need to write out the boundary condition for the remaining two fields, H_φ and D_φ note that for TM_z mode $D_{\varphi 1} = D_{\varphi 2} = 0$.

By solving the boundary condition and eliminating B^- and A^- the dispersion relation for the SSPP modes can be obtained as (12) at the bottom of the page. shown in (13) at the bottom of the page.

By finding the eigenvalues of (12), the dispersion diagram for hybrid modes can be obtained. For special cases, if there is just TM_z modes inside the waveguide, the (12) reduces to (14) at the bottom of the page.

Region 1:

$$\begin{bmatrix} D_\rho \\ D_\varphi \\ D_z \end{bmatrix} = \sum_{m=-M}^{M} \begin{bmatrix} B_m \frac{N}{\rho} I_N(k_\rho \rho)\cos(N\varphi) e^{-ik_z^m z} \\ B_m k_\rho I_N(k_\rho \rho)\sin(N\varphi) e^{-ik_z^m z} \\ 0 \end{bmatrix}$$
$$\begin{bmatrix} H_\rho \\ H_\varphi \\ H_z \end{bmatrix} = \sum_{m=-M}^{M} \begin{bmatrix} -B_m i k_\rho k_z^m I_N'(k_\rho \rho)\sin(N\varphi) e^{-ik_z^m z} \\ B_m \frac{N}{\rho} i k_z^m I_N(k_\rho \rho)\cos(N\varphi) e^{-ik_z^m z} \\ B_m\left(k^2 - k_z^{m^2}\right) I_N(k_\rho \rho)\sin(N\varphi) e^{-ik_z^m z} \end{bmatrix} \tag{8}$$

Region 2:

$$\begin{bmatrix} D_\rho \\ D_\varphi \\ D_z \end{bmatrix} = \begin{bmatrix} \frac{N}{\rho}\left(\mathrm{B}^+ H_N^{2'}(k_{\rho_2}\rho) + \mathrm{B}^- H_N^{1'}(k_{\rho_2}\rho)\right)\cos(N\varphi)\sin\left(\frac{n\pi}{a} z\right) \\ k_{\rho_2}\left(\mathrm{B}^+ H_N^{2'}(k_{\rho_2}\rho) + \mathrm{B}^- H_N^{1'}(k_{\rho_2}\rho)\right)\sin(N\varphi)\sin\left(\frac{n\pi}{a} z\right) \\ 0 \end{bmatrix}$$
$$\begin{bmatrix} H_\rho \\ H_\varphi \\ H_z \end{bmatrix} = \begin{bmatrix} \frac{n\pi}{a} k_{\rho_2}\left(\mathrm{B}^+ H_N^2(k_{\rho_2}\rho) + \mathrm{B}^- H_N^1(k_{\rho_2}\rho)\right)\sin(N\varphi)\cos\left(\frac{n\pi}{a} z\right) \\ -\frac{N}{\rho}\frac{n\pi}{a}\left(\mathrm{B}^+ H_N^{2'}(k_{\rho_2}\rho) + \mathrm{B}^- H_N^{1'}(k_{\rho_2}\rho)\right)\cos(N\varphi)\cos\left(\frac{n\pi}{a} z\right) \\ k_{\rho_2}\left(\mathrm{B}^+ H_N^{2'}(k_{\rho_2}\rho) + \mathrm{B}^- H_N^{1'}(k_{\rho_2}\rho)\right)\sin(N\varphi)\sin\left(\frac{n\pi}{a} z\right) \end{bmatrix}. \tag{9}$$

$$\begin{bmatrix} \sum_{m=-M}^{M} A_m k_\rho \frac{I_N'(k_\rho R_1)}{I_N(k_\rho R_1)} + 1 & \sum_{m=-M}^{M} \frac{N B_m C_m}{A\ R_1} I_N'(k_\rho R_1) \\ \sum_{m=-M}^{M} \frac{A_m C_m k_\rho}{B\ \omega R_1} N k_z I_N(k_\rho R_1) & \sum_{m=-M}^{M} \frac{B_m C_m k_\rho I_N'(k_\rho R_1)}{k_{\rho_2}\frac{2a}{\pi}} - 1 \end{bmatrix} \begin{bmatrix} A^+ \\ B_+ \end{bmatrix} = \begin{bmatrix} 0 \\ 0 \end{bmatrix} \tag{12}$$

$$\begin{aligned} A_m &= \frac{-k_{\rho 2}}{k_\rho} \frac{\left(H_N^1(k_{\rho_2}R_2) H_N^2(k_{\rho_2}R_1) - H_N^2(k_{\rho_2}R_2) H_N^1(k_{\rho_2}R_1)\right)}{\left(H_N^1(k_{\rho_2}R_2) H_N^{2'}(k_{\rho_2}R_1) - H_N^2(k_{\rho_2}R_2) H_N^{1'}(k_{\rho_2}R_1)\right)} C_m^2 \\ B_m &= \frac{k_{\rho_2}}{k_\rho} \frac{\left(H_N^1(k_{\rho_2}R_2) H_N^{2'}(k_{\rho_2}R_1) - H_N^2(k_{\rho_2}R_2) H_N^{1'}(k_{\rho_2}R_1)\right)}{\left(H_N^1(k_{\rho_2}R_2) H_N^2(k_{\rho_2}R_1) - H_N^2(k_{\rho_2}R_2) H_N^1(k_{\rho_2}R_1)\right)} C_m^2 \\ A &= H_N^1(k_{\rho_2}R_2) H_N^2(k_{\rho_2}R_1) - H_N^2(k_{\rho_2}R_2) H_N^1(k_{\rho_2}R_1) \\ B &= H_N^1(k_{\rho_2}R_2) H_N^{2'}(k_{\rho_2}R_1) - H_N^2(k_{\rho_2}R_2) H_N^{1'}(k_{\rho_2}R_1) \end{aligned} \tag{13}$$

$$\sum_{m=-M}^{m=M} \left(\frac{-k_{\rho 2}}{k_\rho}\right) \frac{I_N'(k_\rho R_1)}{I_N(k_\rho R_1)} \frac{\left(H_N^1(k_{\rho_2}R_2) H_N^2(k_{\rho_2}R_1) - H_N^2(k_{\rho_2}R_2) H_N^1(k_{\rho_2}R_1)\right)}{\left(H_N^1(k_{\rho_2}R_2) H_N^{2'}(k_{\rho_2}R_1) - H_N^2(k_{\rho_2}R_2) H_N^{1'}(k_{\rho_2}R_1)\right)} C_m^2 = 1 \tag{14}$$

For the TE_z modes, we have (15) at the bottom of the page, in which the additional variables are defined as

$$\begin{aligned} C_m &= \sqrt{\frac{a}{d}}\mathrm{sinc}\left(\frac{k_z^m a}{2\pi}\right) \\ k_\rho^2 + k_z^{m2} &= n_d^2 k_0^2 \\ k_{\rho 2}^2 + \left(\frac{n\pi}{a}\right)^2 &= n_d^2 k_0^2. \end{aligned} \tag{16}$$

Note that the dispersion equations in (12), (14), and (15) are not only a function of SSPP geometries but also depend on the refractive index of the dielectric inside the SSPP.

It was mentioned before that $a \ll 1$, and the only modes that can propagate inside the grooves are the fundamental modes with $n = 0$ for TM_z and $n = 1$ for TE_z. Based on (8) and (9), there will be no TE_z modes inside grooves; it can exist just at very high frequency in which the wavelength is comparable to the width of grooves. Fortunately this case is not of our interest. Then, we can have TE_z in smooth parts of waveguide but inside the grooves there will be only TM_z modes. The dominant mode in the smooth part of cylindrical waveguide is TE11 and to satisfy the boundary conditions, the TM mode inside the grooves should be TM10.

III. Numerical Results and Discussion

Now that we have developed a mathematical model for the corrugated cylindrical SSPP architectures, the dispersion diagram of such a structure can be obtained by numerically solving (10). Fig. 2(a), for example, shows the dispersion diagram of the azimuthal mode with $N = 0$ for a structure with the dimensions of $R_1 = 120$ μm, $R_2 = 200$ μm, $d = 100$ μm, and $a = 30$ μm. As can be observed, around a normalized frequency of 0.31 (1 THz) the SSPP waveguide can act as a slow wave structure. A transmission band gap exists as the structure reaches its resonance state. In Fig. 2(b) and (c), the field distributions are illustrated at two different frequencies. Fig. 2(d) and (e) shows the magnitude of electric field along the $z-$ direction inside the waveguide at corresponding frequencies in Fig. 2(b) and (c), respectively. It can be seen that most of the energy is concentrated in the center region of the SSPP waveguide when it is off resonance. The EM field confinement within the groove region is clearly demonstrated when the frequency is close to the band gap. In Fig. 2(f), the simulation result obtained by elaborate simulation software packages (HFSS) are shown for the purpose of comparison. As can be observed in both Fig. 2(a) and (f) follows the same behavior versus frequency, but there is a slight difference between our results and the results from HFSS. For example, for the first mode, the normalized cut off frequency based on our model is 0.247, but the HFSS simulation indicates the cut off is 0.245. This discrepancy is due to our assumption that fields inside the grooves are horizontal especially at the boundary of the cylindrical waveguide. However, in real situations these fields try to bend in transition from Region 1 (in our convention) to Region 2. This phenomenon is known as edge effect, as it used to occur at the edge interface of the structure.

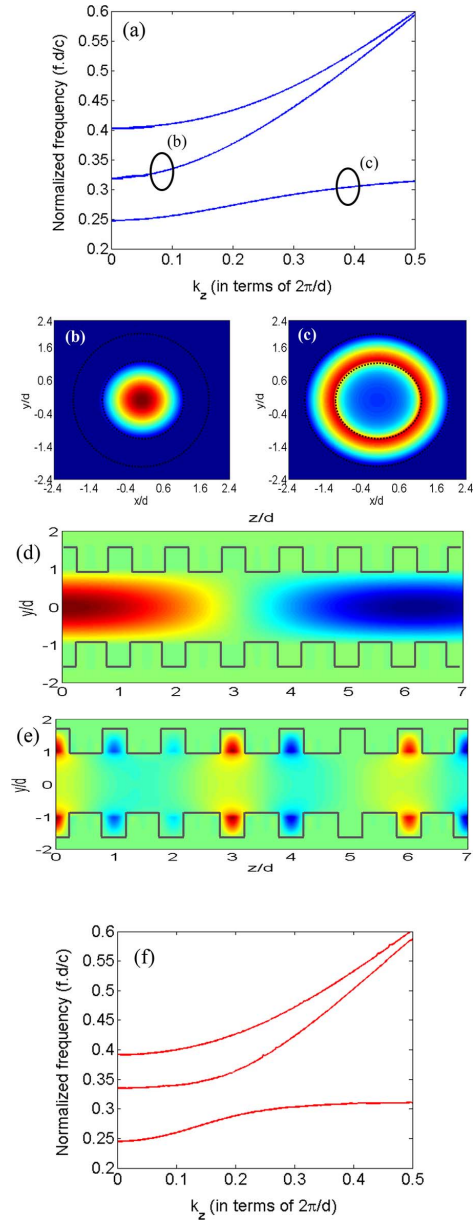

Fig. 2. (a) Dispersion diagram of cylindrical SSPP structure. (b), (c) E_z distribution in cross section of SSPP waveguide at two different frequencies. (d), (e) Electric field magnitude along z-direction inside the waveguide, and (f) dispersion diagram calculated using HFSS.

Also in Fig. 2(a) the behavior of the dispersion diagram of first mode is like the dispersion of surface plasmons along the dielectric metal interface. As a result, we can assume this mode as a SSPP mode with the normalized resonant frequencies of 0.314. The resonant frequency of SSPP waveguide is determined by the resonant frequency of grooves. The two parameters to tailor the resonant frequency of the grooves are width

$$\sum_{m=-M}^{m=M}\left(\frac{k_\rho}{k_{\rho 2}}\right)\frac{I_N(k_\rho R_1)}{I_{N'}(k_\rho R_1)}\frac{\left(H_N^1(k_{\rho_2}R_2)H_N^{2'}(k_{\rho_2}R_1) - H_N^2(k_{\rho_2}R_2)H_N^{1'}(k_{\rho_2}R_1)\right)}{\left(H_N^1(k_{\rho_2}R_2)H_N^2(k_{\rho_2}R_1) - H_N^2(k_{\rho_2}R_2)H_N^1(k_{\rho_2}R_1)\right)}\frac{C_m^2}{\frac{\pi}{2a}} = 1 \tag{15}$$

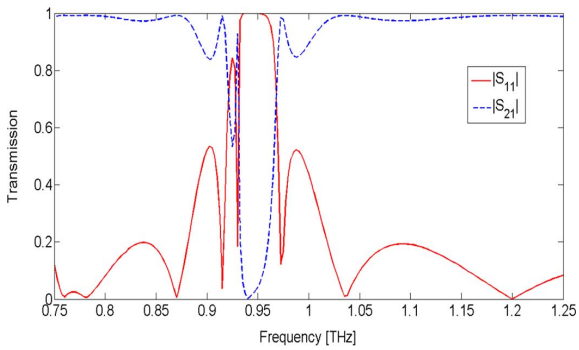

Fig. 3. Transmission characteristic of cylindrical waveguide for $R_1 = 120\ \mu$m $R_2 = 200\ \mu$m, $d = 100\ \mu$m, and $a = 30\ \mu$m.

and height. In our case, the height is much larger than the width. As a result, the resonance along the width occurs in smaller wavelengths compared to the resonance along the height. As our wavelength of interest is comparable to the height, by adjusting the height of the grooves we can control the resonant frequency. As it was mentioned prior, the dominant modes in resonator are TM modes. Thus the resonant frequency can be approximated by using the conventional formula for TM resonant frequency of ring resonators.

For the purpose of comparison, the transmission characteristics of the cylindrical SSPP waveguide is calculated using HFSS and is included here in Fig. 3. The dimensions of SSPP waveguide under investigation are $R_1 = 120\ \mu$m, $R_2 = 200\ \mu$m, $d = 100\ \mu$m and $a = 30\ \mu$m. Based on Fig. 3 a band gap around $f = 0.95$ THz is clearly observed, which is in agreement with the result we obtained by applying our analytical model in Fig. 2.

In Fig. 4, the dispersion diagram for different azimuthal modes ($N = 1{\sim}4$) is illustrated. Dimensions of the waveguide in this case remain the same as the structure studied in Fig. 2. It can be observed that with higher order azimuthal mode, the dispersion curve becomes closer to the light line. As a result, the slow-wave propagation of the input signal in such mode will be observed at slightly higher frequency.

Fig. 4(b) shows E_z intensity at certain frequency below the light line for $N = 4$ and $N = 1$ which is obtained using our analytical modeling. It can be seen that a great portion of the power is confined in the resonators.

Fig. 5, on the other hand, shows the dispersion diagram for first azimuthal mode and different groove dimensions. Other waveguide dimensions in Fig. 5 are kept as $R_1 = 120\ \mu$m, $d = 100\ \mu$m and $a = 30\ \mu$m. It is seen in Fig. 5 that larger groove size in general results in lowered dispersion curves. In addition, narrower passing band is also observed as the groove becomes larger. An intuitive explanation to this phenomenon is the more significant mismatch between the two waveguiding sections in this scenario, which makes it more susceptible to any frequency shift from the transmission maximum.

IV. Polarization Controller

In this section, by inserting the anisotropic dielectric material inside the SSPP waveguide, a polarization rotator is constructed. In Section II, it has been discussed that the (14) is a function of refractive index. This means that by changing the refractive

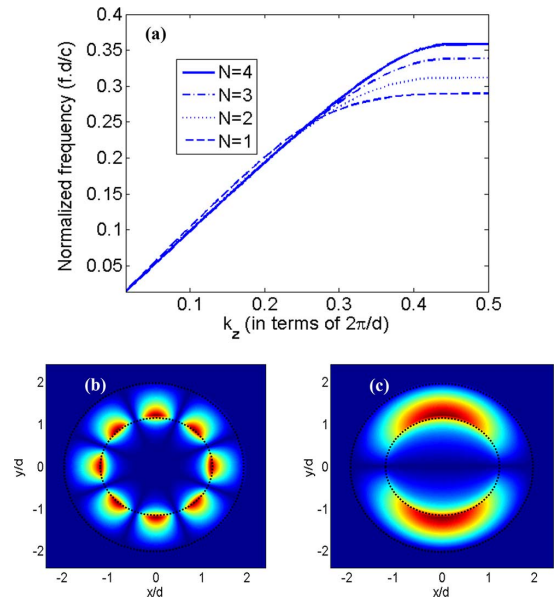

Fig. 4. Dispersion diagram for different azimuthal modes. E_z distribution in cross section of SSPP waveguide for (b) azimuthal mode $N = 4$ and normalized frequency of 0.3537 (c) azimuthal mode $N = 4$ and normalized frequency of 0.3218.

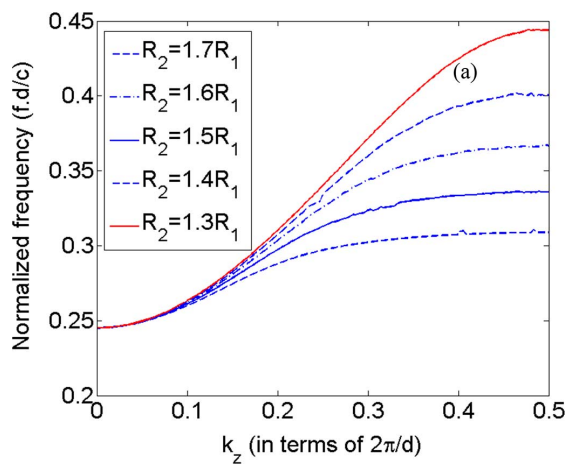

Fig. 5. Dispersion diagram for first azimuthal mode with different groove height.

index inside the waveguide, the propagation constant can be tuned; if the refractive indices in the x and y direction are not equal, each electric component in the x and y direction will experience a different propagation constant. As a result, if we expand the input polarization in terms of the x and y polarization state, it is possible to insert phase difference between these two components along the propagation path. This can lead to the polarization state change which is valid if the polarization state of the input wave can be determined. Fig. 6 shows how electric field direction evolves while propagating.

Fig. 7 shows the electric fields inside the circular waveguide. As can be seen, in the circular waveguide the electric fields at dominant mode are not particularly in a specific direction, but it is possible to assume that they are mostly in a certain direction (in this case in $y = -x$ direction).

Fig. 8 shows the dispersion diagram of the SSPP waveguide for two different sets of refractive indices:

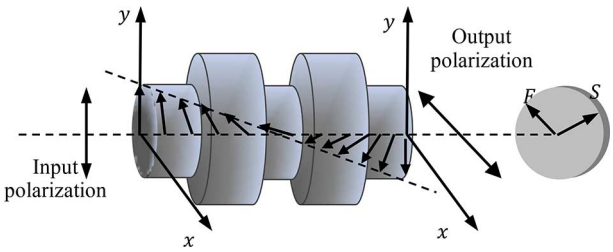

Fig. 6. Schematic view of the rotation of electric field inside the waveguide.

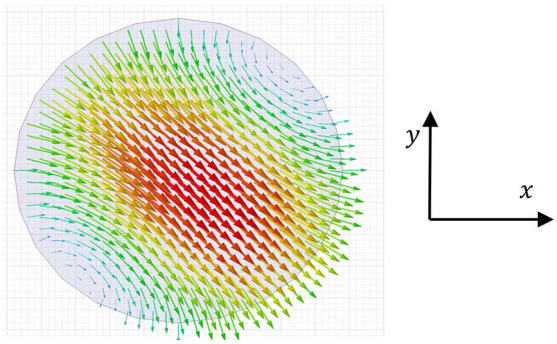

Fig. 7. Polarization of electric field inside the circular waveguide.

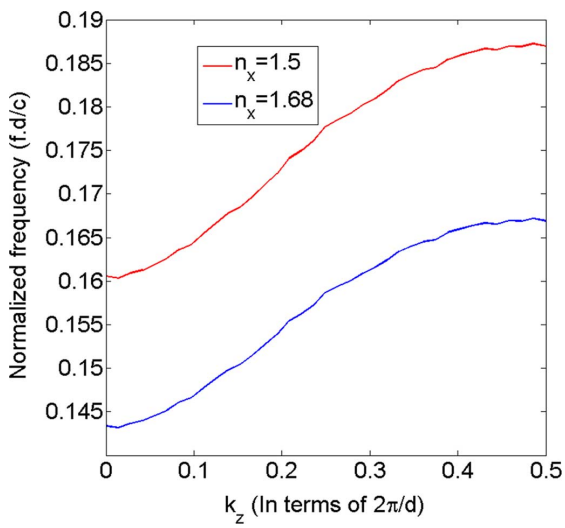

Fig. 8. The dispersion diagram of the same SSPP for two different sets of refractive indices: $(n_x, n_y, n_z) = (1.501, 1.501, 1.501)$ and $(1.501, 1.68, 1.501)$.

$(n_x, n_y, n_z) = (1.501, 1.501, 1.501)$ and $(1.501, 1.68, 1.501)$. The dimensions are $R_1 = 120\ \mu$m, $R_2 = 200\ \mu$m, $d = 100\ \mu$m and $a = 20\ \mu$m. As can be seen, if the operation frequency is in the flat part of dispersion diagram, where the behavior of the dispersion diagram is like the dispersion of surface plasmons along the dielectric metal interface, the phase different between the x and y electric components compare to the conventional circular waveguide would be greater. Then the required waveguide length to evolve the polarization state of the input signal would be smaller.

Fig. 9(a) shows the polarization of electric field inside the SSPP waveguide for $n_x = n_y = n_z = 1.501$ at 0.550 THz. As the dominant mode in the SSPP waveguide is for $N = 1$, then, if for example the input electric fields are in the x direction, the

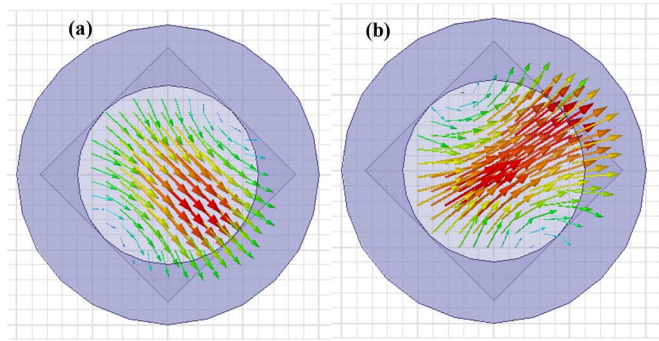

Fig. 9. The polarization of electric field inside the SSPP waveguide for $n_x = n_y = n_z = 1.501$ at .550 THz.

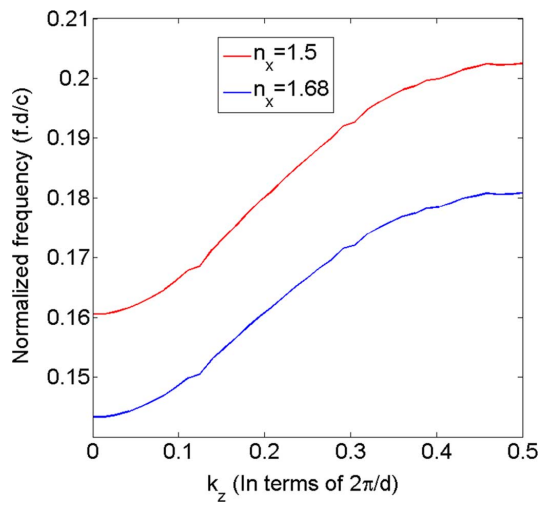

Fig. 10. The dispersion diagram of SSPP for two different sets of refractive indices: $(n_y, n_y, n_z) = (1.501, 1.501, 1.501)$ and (1.501, 1.68, 1.501).

most part of the power will be along the E_x. Then n_x will be seen inside the waveguide. Therefore to find the dispersion diagram for SSPP waveguide with anisotropic dielectric inside it, it is possible to use the (14) in this case. To change the horizontal polarization to vertical state or vice versa, it is needed at first to decompose the input wave into vertical and horizontal polarization, respectively. Then, by inserting 180 degree phase change between them, the polarization state will rotate.

To simulate this process in HFSS it is necessary at first to control the input polarization. To this goal, the excitation of SSPP is done by a rectangular waveguide. This will forcefully define the input polarization. To decompose the input polarization into two polarization states, it is just enough to rotate the rectangular waveguide in respect to the x or y axis.

Fig. 9(b) shows output polarization for the two set of refractive indices of Fig. 8. The length of linear polarization rotator is about 5 periods. The length of the SSPP waveguide to rotate the polarization can be calculated using the following simple formula:

$$l = \frac{\pi}{\beta_2 - \beta_1} \tag{16}$$

In the above, β_2 and β_1 are propagation constants in two refraction indices. To change the horizontal polarization to circular or elliptical state, the 180 degrees of phase change between x and y elements of electric fields should be reduced to

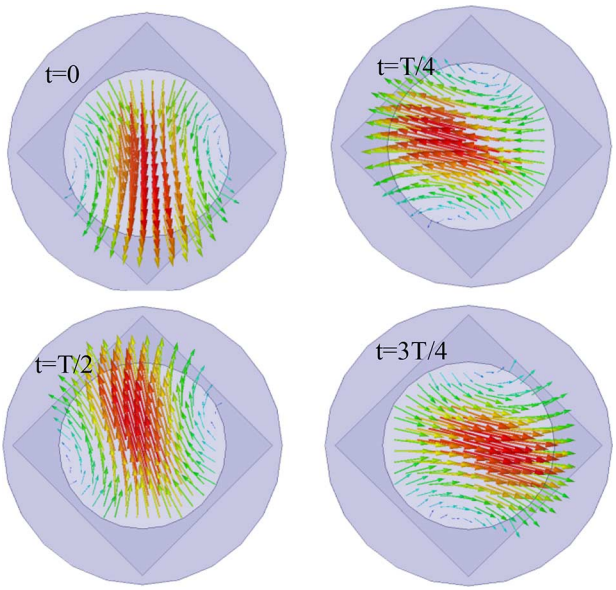

Fig. 11. Rotation of electric field inside the SSPP waveguide for different times at 0.510 THz.

90 degrees. Then in (16) the length of the waveguide just need to be half of previous one. Fig. 10 shows the dispersion diagram of SSPP waveguide. The dimensions are $R_1 = 120\ \mu$m, $R_2 = 220\ \mu$m, $d = 100\ \mu$m, and $a = 20\ \mu$m. The length of circular polarization rotator is about 3 periods.

Fig. 11 shows output polarization for the SSPP waveguide with dispersion diagram shown in Fig. 10. The electric fields are shown in for different time slots. As can be seen the output field's direction is rotating in time. It is worthy to note that if the calculated length was not the integer multiplicand of the periodicity, then the simulation result may be a little bit different from what was expected. In that case, some tuning is required to get the desired result.

V. Conclusion

In this paper, propagation of spoof surface plasmon polariton along periodically grooved cylindrical waveguide comprising anisotropic dielectric has been investigated and mathematical equations for dispersion have been derived. It has been demonstrated that the propagation of SSPP signals can be controlled by modulating the refractive index of dielectric material. The dependence of the band diagrams on the width and depth of the grooves has been explored. It has been shown that the proposed structure can be used as a polarization rotator by engineering the refractive index of inside dielectric. This research on the polarization rotator can be utilized to design THz Boolean logic, such as AND or XOR gates [25].

References

[1] D. M. Mittleman, R. H. Jacobsen, and M. C. Nuss, "T-ray imaging," *IEEE J. Sel. Topics Quantum Electron.*, vol. 2, no. 3, pp. 679–692, May/Jun. 1996.
[2] P. H. Siegel, "Terahertz technology," *IEEE Trans. Microw. Theory Techn.*, vol. 50, no. 3, pp. 910–928, Mar. 2002.
[3] Z. Xu and P. Mazumder, "Bio-sensing by Mach–Zehnder interferometer comprising doubly-corrugated spoofed surface plasmon polariton (DC-SSPP) waveguide," *IEEE Trans. THz Sci. Technol.*, vol. 2, no. 4, Jul. 2012.
[4] R. Kohler *et al.*, "Terahertz semiconductorheterostructure laser," *Nature*, vol. 417, pp. 156–159, 2002.
[5] R. Mendis and D. Grischkowsky, "Plastic ribbon THz waveguides," *J. Appl. Phys.*, vol. 88, pp. 4449–4451, 2000.
[6] W. Zhu, A. Agrawal, and A. Nahata, "Planar plasmonic terahertz guided-wave devices," *Opt. Express*, vol. 16, p. 6216, 2008.
[7] G. Kumar, A. Cui, S. Pandey, and A. Nahata, "Planar terahertz waveguides based on complementary split ring resonators," *Opt. Express*, vol. 19, p. 1072, 2011.
[8] N. Talebi and M. Shahabadi, "Spoof surface plasmons propagating along a periodically corrugated coaxial waveguide," *J. Phys. D: Appl. Phys.*, vol. 43, 2010.
[9] M. Gong, T. Jeon, and D. Grischkowsky, "THz surface wave collapse on coated metal surfaces," *Opt. Express*, vol. 17, no. 19, pp. 17088–17101, 2009.
[10] T.-I. Jeon and D. Grischkowsky, "THz zenneck surface wave (THz surface plasmon) propagation on a metal sheet," *Appl. Phys. Lett.*, vol. 88, no. 6, 2006, Art no. 061113.
[11] G. Gallot, S. P. Jamison, R. W. Mcgowan, and D. Grischkowsky, "Terahertz waveguides," *J. Opt. Soc. Am. B.*, vol. 17, no. 5, pp. 851–863, 2000.
[12] V. Astley, J. Scheiman, R. Mendis, and D. M. Mittleman, "Bending and coupling losses in terahertz wire waveguides," *Opt. Lett.*, vol. 35, no. 4, pp. 553–555, 2010.
[13] F. Yang, J. R. Sambles, and G. W. Bradberry, "Long-range surface modes supported by thin films," *Phys. Rev. B*, vol. 44, no. 11, pp. 5855–5872, 1991.
[14] G. Gallot, S. P. Jamison, R. W. McGowan, and D. Grischkowsky, "Terahertz waveguides," *J. Opt. Soc. Amer. B*, vol. 17, pp. 851–863, 2000.
[15] S. P. Jamison, R. W. McGowan, and D. Grischkowsky, "Single-mode waveguide propagation and reshaping of sub-ps terahertz pulses in sapphire fiber," *Appl. Phys. Lett.*, vol. 76, pp. 1987–1989, 2000.
[16] F. J. Garcia-Vidal, L. Mart'in-Moreno, and J. B. Pendry, "Surfaces with holes in them: New plasmonic metamaterials," *J. Opt. A: Pure Appl. Opt.*, vol. 7, pp. S97–101, 2005.
[17] K. Wang and D. M. Mittleman, "Metal wires for terahertz wave guiding," *Nature*, vol. 432, pp. 376–379, 2004.
[18] J. B. Pendry, L. Martin-Moreno, and F. J. Garcia-Vidal, "Mimicking surface plasmons with structured surfaces," *Science*, vol. 305, pp. 847–848, Aug. 2004.
[19] A. I. Fernandez-Domınguez, L. Martın-Moreno, F. J. Garcıa-Vidal, S. R. Andrews, and S. A. Maier, "Spoof surface plasmon polariton modes propagating along periodically corrugated wires," *IEEE J. Sel. Topics Quantum Electron.*, vol. 14, no. 6, pp. 1515–1521, Nov./Dec. 2008.
[20] K. Song and P. Mazumder, "Active terahertz spoof surface plasmon polariton switch comprising the perfect conductor metamaterial," *IEEE Trans. Electron Devices*, vol. 56, no. 11, pp. 2792–2799, Nov. 2009.
[21] K. Song and P. Mazumder, "Dynamic terahertz spoof surface plasmon-polariton switch based on resonance and absorption," *IEEE Trans. Electron Devices*, vol. 58, no. 7, pp. 2172–2176, Jul. 2011.
[22] Z. Xu, K. Song, and P. Mazumder, "Analysis of doubly corrugated spoof surface plasmon polariton (DC-SSPP) structure with sub-wavelength transmission at THz frequencies," *IEEE Trans. THz Sci. Technol.*, vol. 2, no. 3, pp. 345–354, May 2012.
[23] S. A. Maier, S. R. Andrews, L. Martín-Moreno, and F. J. Garcí-Vidal, "Terahertz surface plasmon-polariton propagation and focusing on periodically corrugated metal wires," *Phys. Rev. Lett.*, vol. 97, 2006, Art no. 176805.
[24] F. Zhang *et al.*, "Magnetic control of negative permeability metamaterials based on liquid crystals," *Appl. Phys. Lett.*, vol. 92, no. 19, p. 193, May 2008, 104–3.
[25] Y. A. Zaghloul and A. R. M. Zaghloul, "Complete all-optical processing polarizationbased binary logic gates and optical processors," *Opt. Express*, vol. 14, no. 21, Oct. 2006.

Mahdi Aghadjani received the B.S. and M.S. degrees in electrical engineering from Iran University of Science and Technology and University of Tehran, respectively, and is currently working toward the Ph.D. degree as a Graduate Student Research Assistant in the Electrical Engineering and Computer Science Department.

His current research interests include designing optical and THz devices.

Pinaki Mazumder (S'84–M'87–SM'95–F'99) received the Ph.D. degree from the University of Illinois at Urbana-Champaign, Urbana, IL, USA, in 1988.

He was the Lead Program Director with the Emerging Models and Technologies Program, University of Michigan, Ann Arbor, MI, USA, through the U.S. National Science Foundation. He has served in Industrial Research and Development Centers, including AT&T Bell Laboratories, Murray Hill, NJ, USA, where he started the CONES Project entitled the first C modeling-based VLSI synthesis tool, and India's premiere electronics company, Bharat Electronics Ltd., Bangalore, India, in 1985, where he had developed several high-speed and high-voltage analog integrated circuits intended for consumer electronics products. He is currently a Professor with the Department of Electrical Engineering and Computer Science, University of Michigan. He has authored more than 200 technical papers and four books on various aspects of very-large-scale integration (VLSI) research works. His current research interests include current problems in nanoscale CMOS VLSI design, CAD tools, and circuit designs for emerging technologies, including Quantum MOS and resonant tunneling devices, semiconductor memory systems, and physical synthesis of VLSI chips.

Dr. Mazumder is a Fellow of the American Association for the Advancement of Science (2008). He was a recipient of the Digital's Incentives for Excellence Award, BF Goodrich National Collegiate Invention Award, and Defense Advanced Research Projects Agency Research Excellence Award.